A methodology for optimal laminar flow control: Application to the damping of Tollmien–Schlichting waves in a boundary layer

Christophe Airiau, Alessandro Bottaro, Steeve Walther, and Dominique Legendre
Institut de Mécanique des Fluides de Toulouse, Allée du Professeur Camille Soula, 31400 Toulouse, France

(Received 24 July 2001; accepted 29 January 2003; published 1 April 2003)

A methodology for determining the optimal steady suction distribution for the delay of transition in a boundary layer is presented. The flow state is obtained from the coupled system of boundary layer equations and parabolized stability equations (PSE), to account for the spatially developing nature of the flow. The wall suction is defined by an optimal control procedure based on the iterative solution of the equations for the state and the dual state; the latter is available from the adjoint boundary layer equations and the adjoint PSE. The technique is applied to the control of two-dimensional Tollmien–Schlichting (TS) waves. Results show that the onset of the instability can be significantly postponed and/or the growth rate considerably reduced by applying an appropriate suction through the whole wall length, in a wide frequency band. Control over panels of finite length completes the study and brings useful, preliminary information on the practicality of the approach in view of implementation. Finally, a simplified methodology which does not rely on the PSE is discussed, based on the minimization of the shape factor. Satisfactory results are achieved with this simpler approach which might, thus, constitute a method of choice when results are needed rapidly, i.e., during on-line control of TS waves. © *2003 American Institute of Physics.*
[DOI: 10.1063/1.1564605]

I. INTRODUCTION

Laminar flow control (LFC) is an old technique in aeronautics (cf. the excellent recent review by Joslin[1]), introduced in the 1930s when the realization came about that a thinner boundary layer is less prone to destabilization to infinitesimal disturbances of the Tollmien–Schlichting (TS) type. Since the laminar skin friction drag can be up to 90% smaller than that in the presence of turbulent flow, the economical advantage of delaying transition is evident. Among the methods adopted to achieve a thinner base flow, the one which has attracted most attention is that based on the suction of fluid through the wall, over all or over portion(s) of the surface, by employing porous plates, suction panels, or other techniques.

In this paper a LFC methodology based on optimal control theory is proposed and validated for the case of two-dimensional TS waves over a flat surface. The procedure is of general nature and can be extended without conceptual modifications to the case of boundary layers over curved surfaces subject to instability waves other than TS. The only limitation is that both base flow and disturbances should develop slowly in the direction(s) parallel to the wall, so that parabolic equations can be established to govern their evolution. Clearly then, the suction applied must be sufficiently ''well-behaved'' not to modify the parabolic nature of the boundary layer equations (BLE). The disturbances are treated by employing the parabolized stability equations (PSE), a system which has already been applied successfully to a large variety of flow cases (cf. Herbert[2] for a recent review). The optimal control procedure rests on the definition of a dual state, which represents the solution of an adjoint system of equations (for both the basic flow and the disturbances). Adjoint equations have recently attracted the increased attention of fluid dynamicists, for a number of applications ranging from flow receptivity to shape optimization, from optimal perturbations to meteorology (the book by Marchuk[3] and the proceedings of a recent workshop on adjoint systems[4] provide but a view of some developments in the field).

Studies on suction-based-LFC can be traced back to the early experiments by Ludwig Prandtl, some one-hundred years ago. He considered the flow past a cylinder and applied suction on one side of the cylinder wall to prevent separation; as a consequence drag was markedly reduced as opposed to the case without suction. The first theoretical study on the effect of suction in a boundary layer is due to Schlichting.[5] By applying uniform suction over an infinite flat plate he determined the ensuing asymptotic velocity profile. Later researchers demonstrated that boundary layers with suction are more stable than the Blasius boundary layer to two-dimensional TS waves (for a full account the reader is referred to the synthesis by Stuart[6]). Interestingly it became customary to represent the critical Reynolds number of the flow as a function of the shape factor H; the collapse of the data corresponding to many different forms of suction onto a single line led Stuart to state that in boundary layers, ''to a reasonable approximation, the critical Reynolds number for any velocity profile is a function of H only.'' A confirmation of this statement is also given by Schlichting.[7] Schlichting also computed the uniform suction velocity necessary to maintain the flow laminar throughout the whole length of the plate; such a value is $V_W = 1.2 \times 10^{-4}$ in outer velocity scale.

Recent works on the subject of optimal control of insta-

bility waves abound in the literature. A significant paper is that by Joslin *et al.*,[8] who proposed a methodology for the determination of suction for drag reduction in a system modeled by the Navier–Stokes equations. The optimality system is ''closed'' by the adjoint Navier–Stokes equations. The mathematics behind the approach, based on Lagrange multipliers, can be found in Gunzburger.[9] The same approach has been followed by Cathalifaud and Luchini[10] in their study of the optimal control of streaks and vortices in flat and curved boundary layers. Also Walther *et al.*[11] employed the Lagrange multiplier formalism to study the optimal control of TS waves in a developing boundary layer. In their work they focused on the control of the instability wave, i.e., the base flow was fixed and the controller acted at the amplitude level of the disturbances. The adjoint PSE equations (APSE) were derived and employed for the purpose, and a successful annihilation of the disturbance wave was achieved (the formidable technological challenge of how to implement the theoretically predicted blowing/suction distribution was not dealt with in the last two papers cited, but it clearly represents the stumbling issue for experimentalists involved in turning theoretical predictions into practice).

The APSE lie at the heart of some of the work described here. They represent a system of backward parabolic equations, the integration of which yields receptivity/sensitivity functions[12] that provide the response of the boundary layer to forcing at the inflow, at the wall or within the flow domain. (Both PSE and APSE are only nearly parabolic. This fact will be briefly discussed further on.) Activities on adjoint equations for receptivity purposes appear to have been initiated in Russia in the 1980s;[13] a flurry of new results for both local and nonlocal stability problems have been published in the last few years.[14–22] In the present work the APSE represent but a step of the optimization process. Adjoint equations arise naturally in variational procedures; for example, they have been employed in the study by Balakumar and Hall[23] focused on determining the optimal suction distribution for the reduction of the N factor, for instability waves growing on top of the Blasius and the Hiemenz flows.

In closing this section we note that an approach similar to ours is being pursued at the same time in Sweden,[24,25] both groups involved working under the impulse, and with partial support, of the European project ALTTA (Application of Hybrid Laminar Flow Technology on Transport Aircrafts).

II. PROBLEM MODELING

We consider a two-dimensional flow above a flat plate between $x=x_0$ and $x=x_f$; x_0 is located upstream of branch I of the neutral curve and x_f downstream. A normal suction is applied at the wall $(y=0)$ over a streamwise domain Γ_C included in $[x_0,x_f]$ (dimensionless values). The flow state is defined by a mean velocity,

$$\mathbf{Q}(x,y)=[U,V]^T(x,y),$$

and by a disturbance vector,

$$\tilde{\mathbf{q}}(x,y,t)=[\tilde{u},\tilde{v},\tilde{p}]^T(x,y,t).$$

Velocities are scaled by the free stream velocity U_∞ and lengths by $\delta_0(x_0')=\sqrt{\nu x_0'/U_\infty}$, ν being the kinematic viscosity and x_0' the dimensional equivalent of x_0. These characteristic quantities define a Reynolds number $R_{\delta_0}=R_\delta(x_0')=\sqrt{U_\infty x_0'/\nu}$. The evolution of the mean flow is described by Prandtl's equations with classical boundary conditions except for the normal velocity at the wall; in symbolic form

$$\mathcal{L}_{\mathrm{P}}\mathbf{Q}=\mathbf{0}, \tag{1}$$

$$\lim_{y\to+\infty} U(x,y)=1, \quad \mathbf{Q}(x,0)=[0,V_W]^T(x). \tag{2}$$

The system is initialized at $x=x_0$ with the Blasius flow solution. Using this model we implicitly assume that the mean pressure remains unaffected by the wall forcing, i.e., that the magnitude of the wall forcing is of order $R_{\delta_0}^{-1}$. The appropriateness of this assumption is evaluated in Appendix A.

The behavior of TS waves can be well described by the PSE. These linear equations were first proposed by Herbert and Bertolotti[26] and are fully documented in Refs. 27 and 28. The advantages of such an approach are multiple: it allows a spatial resolution of the problem, which is physically more relevant than a temporal approach; the equations are quasiparabolic[29,30] in the streamwise direction so that they can be easily and accurately solved by a numerical marching procedure, and they take into account the streamwise weak dependency of the perturbation mode shapes. The state disturbance vector in the PSE approach reads

$$\tilde{\mathbf{q}}(x,y,t)=\mathbf{q}(x,y)\chi(x)e^{-i\omega t},$$

with $\mathbf{q}=[u,v,p]^T$ and $\chi(x)=\exp(i\int_{x_0}^{x}\alpha(\xi)d\xi)$. The amplitude function $\mathbf{q}$ is slowly varying in x, whereas χ varies rapidly; ω defines a frequency and α is a complex function, whose real and imaginary parts correspond, respectively, to a wave number and an amplification rate.

The linear PSE system can be formally written

$$\mathcal{L}_{\mathrm{PSE}}\mathbf{q}=\mathbf{0},$$

with

$$\mathcal{L}_{\mathrm{PSE}}=\mathcal{A}\frac{\partial}{\partial y}+\mathcal{B}\frac{\partial}{\partial x}+\mathcal{C}+\mathcal{D}\frac{\partial^2}{\partial^2 y}, \tag{3}$$

$$\int_0^{+\infty}\left(\bar{u}\frac{\partial u}{\partial x}+\bar{v}\frac{\partial v}{\partial x}\right)dy=0, \tag{4}$$

the over-bar denoting complex conjugates. Boundary conditions on u and v are homogeneous at the wall and in the free stream. Equation (4) is a closure relation for the determination of α, forcing the amplitude function to vary slowly in the streamwise direction. Even though its choice is arbitrary, a different normalization condition would induce only a small, $\mathcal{O}(R_{\delta_0}^{-2})$, modification to α. The initial conditions are given by the local stability eigenfunctions. All equations, for the base flow and the disturbances, and matrix operators $\mathcal{A}$, $\mathcal{B}$, $\mathcal{C}$, $\mathcal{D}$ are given in Appendix B.

III. OPTIMAL CONTROL

This section describes the optimal control approach pursued. First, the problem of interest here is defined in a general manner. Then, the Lagrange multipliers methodology is explained.

As a first step, some key ''ingredients'' must be identified, i.e.,

(1) the state functions which characterize the problem, here the mean flow $\mathbf{Q}$ and the TS wave $(\mathbf{q},\alpha)$;
(2) the constraints: the Prandtl-PSE problem with its boundary conditions;
(3) the way control is applied: a wall-normal forcing V_W;
(4) the cost functional $\mathcal{J}_0$ which must be extremized.

The choice of $\mathcal{J}_0$ is crucial. Since our objective is to neutralize (or limit the growth of) the TS wave throughout the domain, the cost functional must include an appropriate measure of the perturbation amplitude. Thus, a relevant quantity is the magnitude of the disturbance energy at the final station $x=x_f$,

$$E_f=E(x_f),$$

with

$$E(x)=|\chi|^2\int_0^{+\infty}(\overline{u}u+\overline{v}v)dy.$$

In view of (4) the variation of E with x is related uniquely to the presence of the term $|\chi|^2$. Thus, when x_f is chosen near branch II of the neutral curve, minimizing $E(x_f)$ over a range of frequencies is equivalent to minimizing the N factor defined by

$$N(R_{\delta_0})=\max_{\omega}\left(\frac{1}{2}\log\frac{E}{E(x_{\mathrm{I}})}\right),$$

with x_{I} located on branch I. This coefficient is commonly taken to characterize the transition location of the flow: it is usually admitted that for $N\approx 7$ transition occurs[31] (in a two-dimensional boundary layer). Although the determination of the ''critical'' value of N is purely empirical and does not take into account the inflow disturbances conditions, the so-called e^N method, introduced in the 1950s,[32,33] is still widely used nowadays in the aeronautical industry.

One may argue that choosing E_f as a cost functional does not guarantee *a priori* that the perturbation amplitude would decrease significantly over the whole unstable region. Hence, it may be more convenient to introduced in $\mathcal{J}_0$ the mean value of E over an objective domain Γ_m,

$$E_m=\int_{\Gamma_m}E(x)dx.$$

In general Γ_m may be the whole domain $[x_0,x_f]$ or a portion of it such as, for example, the unstable region of the TS wave under unforced conditions. The final cost functional is then

$$\mathcal{J}_0=k\frac{E_f}{E_f^{\mathrm{unc}}}+(1-k)\frac{E_m}{E_m^{\mathrm{unc}}}+s\int_{\Gamma_C}\left(\frac{dV_W}{dx}\right)^2dx,$$

with k between zero and one depending on the goal we pursue, and the exponent ''unc'' indicating the reference value of the uncontrolled case. The last term in the cost function is introduced to prevent the occurrence of sharp gradients of the wall normal velocity,[34] which could violate the BLE and PSE assumptions. It plays the role of a penalty in the objective functional. In practice the case $s=0$ produces a solution (which may or may not violate the parabolic assumption), and by increasing s this solution is simply smoothened at the outer edges of Γ_C.

A further requirement must be considered: to prevent having an ill-posed problem leading to unbounded solutions, we must ensure that the size of the control remains small so that suction does not affect the mass flux (provoking the so-called *sink effect*). To ensure this we impose the value of the control energy as an additional constraint, i.e.,

$$\int_{\Gamma_C}V_W^2\,dx=E_C, \tag{5}$$

with E_C fixed. The advantages of such an approach are that the parameter E_C has a physical meaning, and that comparisons between different cost functionals can be easily made for a given control energy. Alternatively, we could have chosen to fix the flow rate through the porous wall, or the power consumption of the compressor needed to suck fluid from the wall (the latter quantity being proportional to V_W^3). Taking power of two of the control function has the advantage of yielding a simple linear relation on V_W once functional gradients are set to zero.

The optimal control problem is now stated as follows: *Find the normal velocity at the wall V_W and the state $(\mathbf{Q},\mathbf{q},\alpha)$ which minimize the cost functional $\mathcal{J}_0$ subject to the constraints (1), (2), (3), (4), (5) with appropriate boundary and initial conditions*.

The method used in this paper to solve this control problem is based on Lagrange multipliers, as described, for instance, by Gunzburger.[9] The principle of the method is to transform the constrained optimization problem into an unconstrained one. For this purpose the following inner product is defined,

$$\langle\phi,\psi\rangle=\int_{x_0}^{x_f}\int_0^{+\infty}\overline{\phi}\psi\,dy\,dx.$$

Lagrange multipliers $(\mathbf{Q}^*,\mathbf{q}^*,\lambda^*,\gamma^*,\beta_W^*)$ are then introduced to enforce the constraints and a Lagrangian functional is defined:

$$\mathcal{L}=\mathcal{J}_0-\mathcal{J}_1, \tag{6}$$

with

$$\begin{aligned}\mathcal{J}_1=&\langle\mathbf{Q}^*,\mathcal{L}_{\mathrm{P}}\mathbf{Q}\rangle+\int_{x_0}^{x_f}\lambda^*(x)[V(x,0)-V_W(x)]dx\\&+\beta_W^*\left(E_C-\int_{\Gamma_C}V_W^2\,dx\right)+\langle\mathbf{q}^*,\mathcal{L}_{\mathrm{PSE}}\ \mathbf{q}\rangle\\&+\int_{x_0}^{x_f}\overline{\gamma}^*(x)\int_0^{+\infty}\left(\overline{u}\frac{\partial u}{\partial x}+\overline{v}\frac{\partial v}{\partial x}\right)dy\,dx+\text{c.c.},\end{aligned}$$

where c.c. denotes complex conjugates, needed to ensure that the range of the functional $\mathcal{J}_1$ is the real axis. We will see later that the Lagrange multipliers $\mathbf{Q}^*,\mathbf{q}^*,\lambda^*,\gamma^*$ play the role of adjoint (or dual) variables for the direct variables $\mathbf{Q},\mathbf{q},V_W,\alpha$. β_W^* is the adjoint variable for the control constraint. All arguments of the Lagrangian functional are independent from one another and the optimal control problem can now be stated as:

Find the control V_W*, the state* $(\mathbf{Q},\mathbf{q},\alpha)$ *and the dual state* $(\mathbf{Q}^*,\mathbf{q}^*,\lambda^*,\gamma^*)$ *which render* $\mathcal{L}$ *stationary.*

It should be pointed out that this formulation guarantees only a local extremum; in practice, the numerical results show that a minimum is always found, which satisfies the imposed requirements and produces a strong reduction of the disturbance energy.

The gradient of $\mathcal{L}$ in every direction is forced to zero and this step requires several integrations by parts. Details on how to effect this procedure can be found in Ref. 11. Canceling the gradient of $\mathcal{L}$ with respect to the dual state $(\mathbf{Q}^*,\mathbf{q}^*,\lambda^*,\gamma^*)$ leads to the Prandtl-PSE problem (1,2,3,4). The vanishing of the gradient of $\mathcal{L}$ with respect to the state $(\mathbf{Q},\mathbf{q},\alpha)$ yields the adjoint Prandtl-PSE problem, i.e., in symbolic form

$$\mathcal{L}_{\mathrm{P}}^*\mathbf{Q}^*=\mathbf{S}^*,\quad \mathbf{Q}^*=[A,B]^T,$$

$$\mathcal{L}_{\mathrm{PSE}}^*\mathbf{q}^*=\mathbf{s}^*,\quad \mathbf{q}^*=[u^*,v^*,p^*]^T,$$

$$\frac{dJ}{dx}(x)=\begin{cases}0, & x\notin\Gamma_m\\ (k-1)\dfrac{E(x)}{E_f^{\mathrm{unc}}}, & x\in\Gamma_m,\end{cases}$$

with $(\mathbf{S}^*,\mathbf{s}^*)$ source terms which depend, respectively, on $(\mathbf{Q},\mathbf{q},\mathbf{q}^*,\alpha)$ and $(\mathbf{q},\gamma^*,\alpha)$. $J(x)$ is a function of the direct and adjoint variables and provides a closure relation for the determination of γ^*. The role of $J(x)$ is described, for example, in Refs. 11, 15, 19–22; it is a function related to the receptivity properties of the boundary layer. By construction, the adjoint Prandtl and PSE equations are backward parabolic in x; they are given in Appendix B.

The adjoint equations are subject to homogeneous boundary conditions and are initialized at x_f with

$$A(x_f,y)=\mathbf{0},$$

$$\mathbf{q}^*(x_f,y)=\left(k\frac{\chi\overline{\chi}}{E_f^{\mathrm{unc}}}-\gamma^*\right)\left[0,\frac{v}{U},u\right]^T(x_f,y),$$

$$\gamma^*(x_f)=k\frac{\chi\overline{\chi}}{E_f^{\mathrm{unc}}}\left.\frac{\displaystyle\int_0^{+\infty}\frac{2i\overline{\alpha}}{R_{\delta_0}U}\overline{v}v\,dy}{\displaystyle\int_0^{+\infty}\left(1+\frac{2i\overline{\alpha}}{R_{\delta_0}U}\right)(\overline{u}u+\overline{v}v)dy}\right|_{x_f},$$

$$J(x_f)=k\frac{E(x_f)}{E_f^{\mathrm{unc}}}.$$

Source terms and inhomogeneous terminal conditions stem from the choice of the cost functional (see also Refs. 21 and 25); they are given in Appendix B.

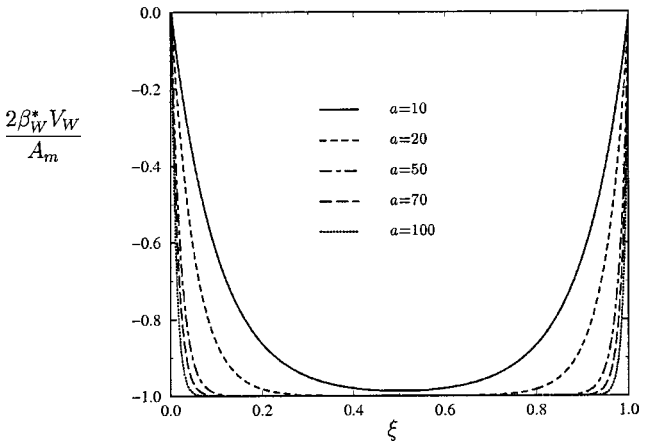

FIG. 1. Model of the suction velocity.

Finally, the vanishing of the gradient of $\mathcal{L}$ with respect to V_W provides a coupling relation between direct and adjoint states. This expression, the *optimality condition*, defines the optimal wall forcing V_W as a function of the adjoint vector $\mathbf{Q}^*$ at the wall. With the cost functional given by Eq. (6), we obtain the ordinary differential equation:

$$\frac{D\mathcal{L}}{DV_W}=2s\frac{d^2V_W}{dx^2}-2\beta_W^*V_W-A(x,0)=0, \tag{7}$$

with the boundary conditions $V_W=0$ at both edges of the control domain Γ_C. $A(x,0)$ is the Lagrange multiplier associated with the continuity equation of the base flow, evaluated at the wall. When $s\neq 0$, the V_W-velocity profile exhibits two ''boundary layers'' at the outer edges of Γ_C. This can be seen by considering a simpler equation where $A(x,0)=A_m$ is fixed to a constant value [for example, the mean value of $A(x,0)$] in a control domain defined by $\Gamma_C=[x_0,x_f]$. The solution of Eq. (7) is in this case

$$V_W(x)=\frac{A_m}{2\beta_W^*}\left[\frac{\cosh a(\xi-0.5)}{\cosh\dfrac{a}{2}}-1\right],$$

$$a^2=\frac{\beta_W^*}{s(x_f-x_0)^2},\quad \xi=\frac{x-x_0}{x_f-x_0}.$$

The model suction velocity is plotted in Fig. 1 for different values of $a=a(\beta_W^*/s,\Gamma_C)$. When β_W^* is fixed, the slope of the wall-normal suction velocity at the boundaries increases with decreasing s. The control profiles calculated by the full equations show a behavior with respect to s which is well modeled by the simple case $A(x,0)$ constant.

In the general case, we define a slope parameter, c_0, given by $s=c_0\beta_W^*$. In practice, c_0 is imposed, and the parameter s is calculated. β_W^*, the Lagrange multipliers associated with the control energy, is found during the iterative process from the constraint (5) and the integration of Eq. (7) over Γ_C:

$$\beta_W^* = \left(\frac{\int_{\Gamma_C} A^2(x,0)\,dx}{4[E_C + c_0 \int_{\Gamma_C} (c_0 V_W''^2 + 2V_W'^2)\,dx]} \right)^{1/2}, \qquad (8)$$

primes denoting derivation with respect to the argument. When $s=0$, the value of β_W^* is given by Eq. (8) with $c_0=0$ and the slope of the wall-normal velocity may go to infinity at the edges of Γ_C. If Γ_C extends to x_f, the sharp gradient of V_W does not occur there, since $A(x_f,0)=0$.

IV. NUMERICAL IMPLEMENTATION

The optimal state is numerically reached by an iterative procedure involving successive integrations of the direct and adjoint equations, according to the following algorithm.

(1) Step 1: Initialization of the PSE problem using the local stability eigen-solutions; on the first iteration, when $n=1$, $V_W^{(n)}$ is set to zero.
(2) Step 2: Solution of the Prandtl problem with $V(x,0)=V_W^{(n)}(x)$.
(3) Step 3: Solution of the PSE problem.
(4) Step 4: Convergence test on the objective functional: if $|\mathcal{J}_0^{(n)}-\mathcal{J}_0^{(n-1)}|/\mathcal{J}_0^{(n)}<\epsilon_0$ then stop, else $n=n+1$; a case is considered well converged when $\epsilon_0=10^{-4}$.
(5) Step 5: Initialization of the adjoint PSE and boundary layer problems using the direct state.
(6) Step 6: Solution of the adjoint PSE problem.
(7) Step 7: Solution of the adjoint Prandtl problem.
(8) Step 8: Update of the wall forcing distribution $V_W^{(n)}$ via the optimality condition and the constraint on the control energy, i.e., $V_W^{(n)}=V_W^{(n-1)}+(\rho/2\beta_W^*)(D\mathcal{L}/DV_W)^{(n-1)}$.
(9) Step 9: Go to step 2.

Although no efforts are made to optimize the relaxation parameter ρ, convergence is rather quick, and is typically reached in about ten iterations. More sophisticated optimization algorithms have been employed, for example, in the work by Pralits *et al.*[25] and can be necessary in other types of optimization problems.

Since the direct and adjoint problems are of the same nature, the same grid and finite difference tools are used for their resolution. The grid is uniform in the x direction (step Δx) and stretched in the y direction, refined near the wall. In the streamwise direction a first-order upwind or downwind, depending of the state, scheme is employed for the PSE-APSE problem and a second-order scheme is used for the direct and adjoint Prandtl's equations. The normal direction is treated by a fourth-order compact scheme [Eq. (7) as well]. The free-stream boundary is located 15 boundary layer thicknesses away from the wall. The closure relations are enforced by a Newton–Raphson procedure. Grid convergence studies have been carried out, and solutions on a mesh of 400 streamwise points and 150 normal points for the case of Fig. 2 are grid-converged (but these are not the minimum numbers of points needed to reach convergence). Further details on the PSE/APSE procedure are given in Ref. 11. It should be noted that, in general, the "best" grid for the PSE does not coincide with the "best" grid for the APSE, where by "best" we mean the coarsest mesh producing grid-converged solutions. All solutions here are obtained with the same (fine) grid for PSE and APSE, and this is simply a convenient choice since calculations proceed very rapidly.

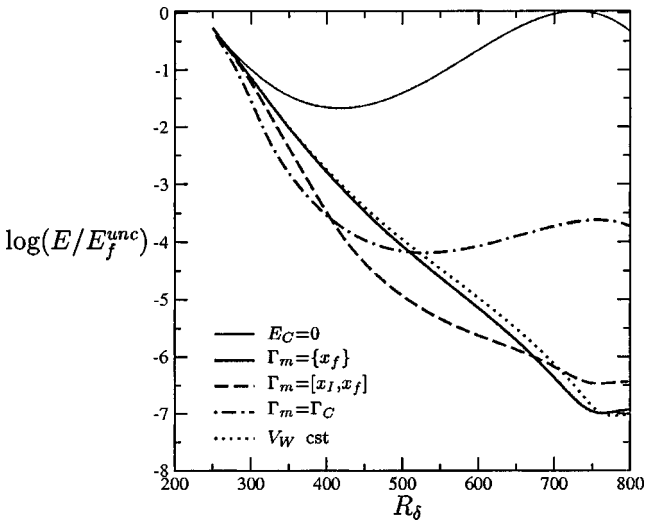

FIG. 2. Disturbance energy for different Γ_m: $F=10^{-4}$, $E_C=5\times10^{-7}$.

The APSE and PSE are nearly parabolic and a numerical instability usually occurs at extremely small streamwise step size, when Δx is lower than $\Delta x_{\min}\approx 1/\mathrm{Real}(\alpha)$. A procedure given in Ref. 29 has been implemented for the PSE and it induces a corresponding modification on the APSE (for details of this technical aspect of the numerical implementation the reader can consult Ref. 25). The case $c_0=0$ of Fig. 7 (with only 50 points in x, no stabilization procedure) produces exactly the same results as the "reference" case of Fig. 2 ($\Gamma_m=\{x_f\}$), which is obtained with the stabilization procedure. We have also found that the minimal step $\Delta x_{\min}$ is nearly the same for the PSE and the APSE. The numerical instability of the PSE has been well known for years;[2,28,30] many techniques have been developed to cope with it and robust codes now exist and are used in practical applications.[2,24,25]

V. RESULTS

The theory is applied for different reduced frequencies F ($F=\omega/R_\delta$) ranging from 10^{-5} to 27×10^{-5}. Unless otherwise stated, the suction domain Γ_C starts at x_0 and stops at x_f.

A first test consists in estimating the influence of the size of the objective domain Γ_m for a given frequency $F=10^{-4}$, with a control energy fixed at $E_C=5\times10^{-7}$, and $c_0=0$. The parameter E_C is chosen to provoke significant wave damping, after several numerical trials and from the rough estimate $E_C\approx(x_f-x_0)\overline{V}_W^2$, where $\overline{V}_W\approx10^{-4}$ (cf. Sec. I); x_0 and x_f are taken such that $R_\delta(x_0)=250$ and $R_\delta(x_f)=750$. In practice, computations are often carried on beyond x_f to follow the further evolution of the TS wave. The variation of $E(x)$ normalized by the value of $E(x_f)$ for the uncontrolled case is plotted in Fig. 2 and the associated optimal forcing profiles are shown in Fig. 3. In the first case (denoted by $\Gamma_m=\{x_f\}$, the "reference" case) the objective is to minimize the disturbance energy at the final station x_f, whereas in the second and third cases Γ_m corresponds, respectively, to

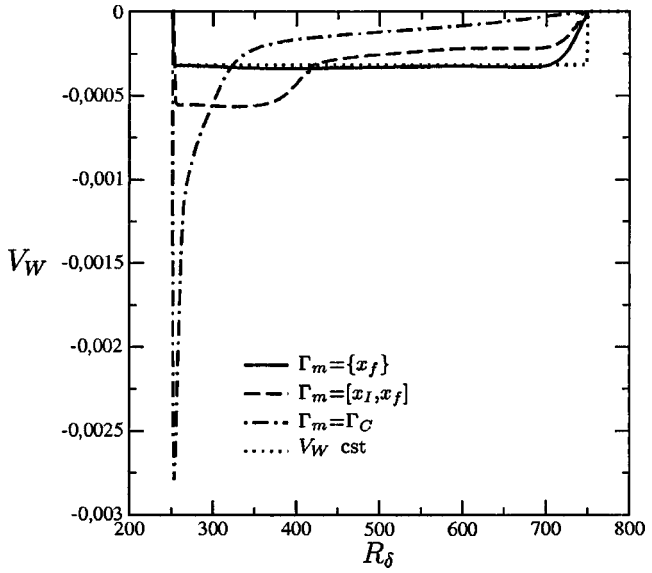

FIG. 3. Optimal wall suction profiles for different Γ_m: $F=10^{-4}$, $E_C=5\times10^{-7}$.

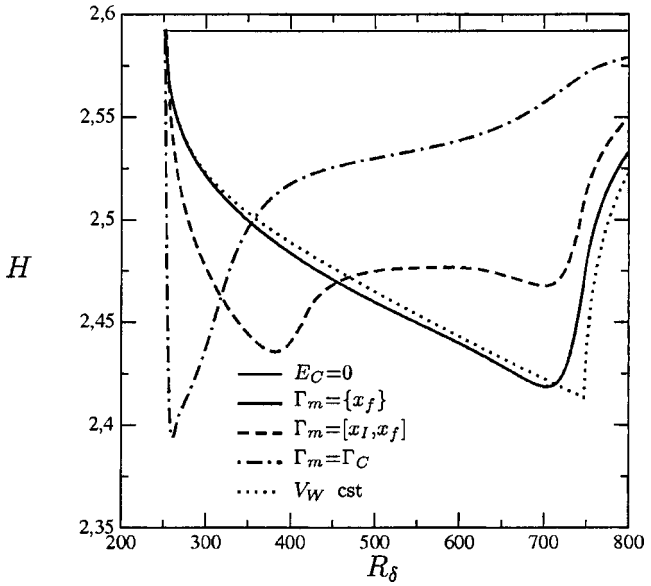

FIG. 4. Optimal shape factors for different Γ_m: $F=10^{-4}$, $E_C=5\times10^{-7}$.

the unstable region [of the uncontrolled case, beginning at $R_\delta(x_I)=419.5$] and to the whole suction domain. In the last case a constant suction distribution V_W with $E_C=5\times10^{-7}$ is applied all along Γ_C. As expected, the smaller perturbation energy at x_f is achieved in the first configuration; the best result in terms of reduction of the mean (along x) energy is given by the third case. It should, however, be noticed that whatever the case, the energy is always reduced very considerably over the entire domain and particularly in the unstable region where $R_\delta>420$. The evolution of the disturbance energy when $\Gamma_m=\{x_f\}$ is almost identical to the case with constant suction. The suction distribution differs considerably according to the objective imposed. The profile in the first case is similar to the case with constant suction. For the second case, suction is mainly localized upstream of Γ_m (here, the stable region of the uncontrolled flow), and for the limit case where $\Gamma_m=\Gamma_C=[x_0,x_f]$ (third case) the control is almost essentially imposed at the entrance of the domain. The effects on the shape factor H and on the growth rate $\sigma=(1/E)(dE/dx)$ of these distributions are evaluated in Figs. 4 and 5. Figure 4 shows that whenever suction is applied, the shape factor is reduced. Furthermore, the variations of H are quite well correlated to those of the corresponding suction profiles, so that the minimum of H is more or less located at the station where suction is most intense. As the evolution of the energy curves indicates, the region where the growth rate is positive is reduced after suction is applied (cf. Fig. 5). When suction is stopped the shape factor increases back to its value without control, whereas the growth rate σ crosses the horizontal axis after a transient period, whose length increases as Γ_m decreases. Figures 3, 6, and 8 show that for $\Gamma_m=\Gamma_C=[x_0,x_f]$, the very strong variation of the wall velocity near x_0 produces a sharp peak on the growth rate evolution, a fact which might contradict the hypotheses at the basis of the PSE. It is hence an unwise (*a posteriori*) choice to select $\Gamma_m=\Gamma_C$. As demonstrated next, adding a term penalizing the square of the streamwise derivative of the control function in the objective functional decreases the steep variation of the suction velocity, leading to smoother growth rate. The appropriateness of Prandtl's equations in representing flows with rapid variations in the vertical velocity is discussed in Appendix A, which presents some comparisons with full Navier–Stokes computations. When comparing to the results by Balakumar and Hall[23] one might be struck by the differences between the control velocities in the two approaches for comparable flow cases. These differences originate primarily from the different cost functionals employed in the two control methodologies.

The effect of varying c_0 is assessed next, for the so-called "reference" case ($\Gamma_m=\{x_f\}$). Figures 6 and 7 show the influence of the slope parameter c_0 on the suction profile and disturbance energy when either the control energy E_C is fixed, or when β_W^* is fixed to the "reference" value (the

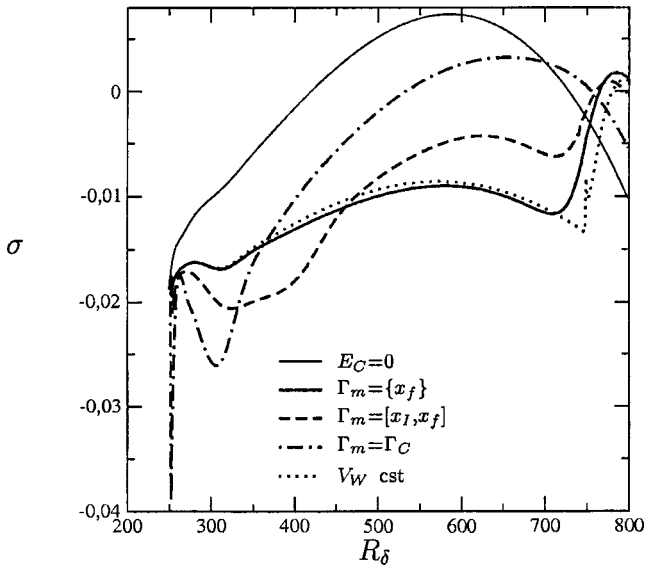

FIG. 5. Optimal growth rate for different Γ_m: $F=10^{-4}$, $E_C=5\times10^{-7}$.

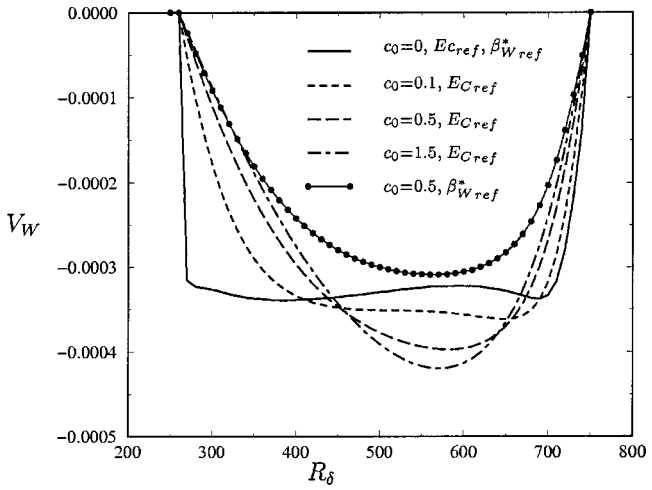

FIG. 6. Optimal wall suction profiles for different values of the slope parameter c_0. $F=10^{-4}$, $E_C=5\times10^{-7}$.

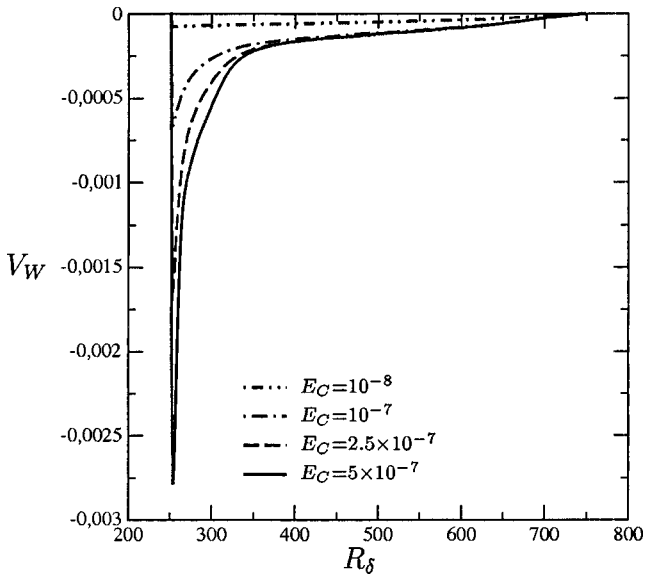

FIG. 8. Optimal wall suction profiles for different E_C: $F=10^{-4}$, $\Gamma_m=\Gamma_C$, $c_0=0$.

legend of the plot indicates which quantity is held fixed). In the first case, the slope of V_W decreases at the edges of Γ_C, but V_W increases locally within the control domain to maintain the contraint on the control energy. As far the disturbance energy curve is concerned, the results are very close among all the configurations examined in Fig. 7. In the second case ($c_0=0.5$, $\beta^*_W=\beta^*_{Wref}$), fixing β^*_W means decreasing the control energy E_C and penalizing the final disturbance energy. Eventually, the control is found to be less efficient. The case $s=0$ provides the most efficient suction profile for any given control energy E_C (cf. Fig. 7). In the remainder of the paper, c_0 is always fixed to zero simply to provide the limiting case scenario as to the reduction of the disturbance energy.

In the figures that follow the influence of the energy E_C is assessed for $\Gamma_m=\Gamma_C=[x_0,x_f]$ and $\Gamma_m=\{x_f\}$, at the frequency $F=10^{-4}$. In the first case (Figs. 8 and 9), the suction distributions always decrease from x_0 to x_f. For a local Reynolds number R_δ greater than 400 there is no significant difference among all suction profiles, except when E_C is equal to 10^{-8}. This results in similar variations of the disturbance energy E downstream of $R_\delta=400$. As the level of E_C increases, the suction is more intense in the close vicinity of x_0, so that E decreases more rapidly at the beginning of Γ_m. When Γ_m is reduced to the last station (Fig. 10), suction is more or less equally spread all over Γ_C, even for a high level of control energy. For the largest value of E_C suction is maximum at the end of the control domain, but even then the profile varies relatively smoothly (cf. Figs. 10 and 11). This quasihomogeneous spreading of the wall velocity permits the employment of a bigger amount of control energy as compared to the case with $\Gamma_m=\Gamma_C$, where sharp peaks at the domain entrance can become quickly of order R_δ^{-1}. One must, however, always weight the cost of controlling the flow against the expected benefits. Since considerable reductions in E are achieved even for small control energies, as Fig. 11 shows, it might be unnecessary to adopt a costly strategy. This is further compounded by the fact that in real

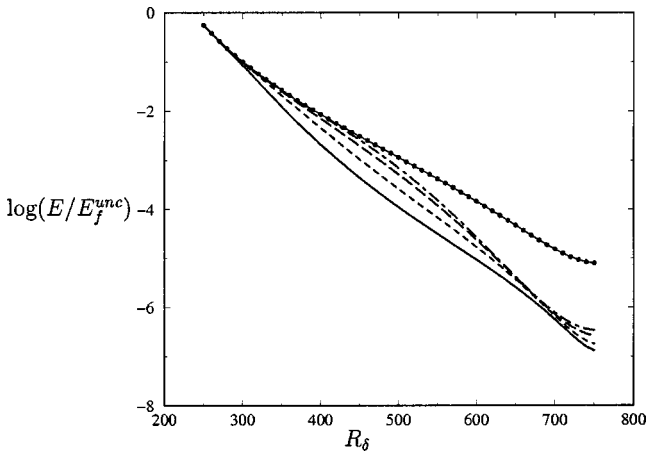

FIG. 7. Disturbance energy for different values of the slope parameter c_0. For caption, see Fig. 6.

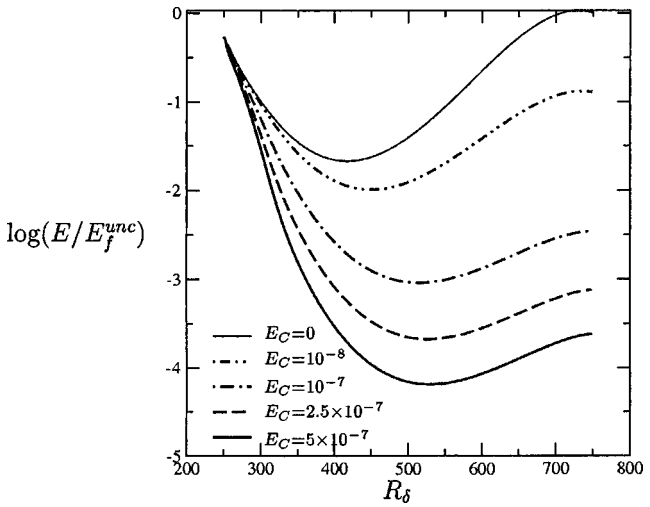

FIG. 9. Optimal disturbance energies for different E_C: $F=10^{-4}$, $\Gamma_m=\Gamma_C$, $c_0=0$.

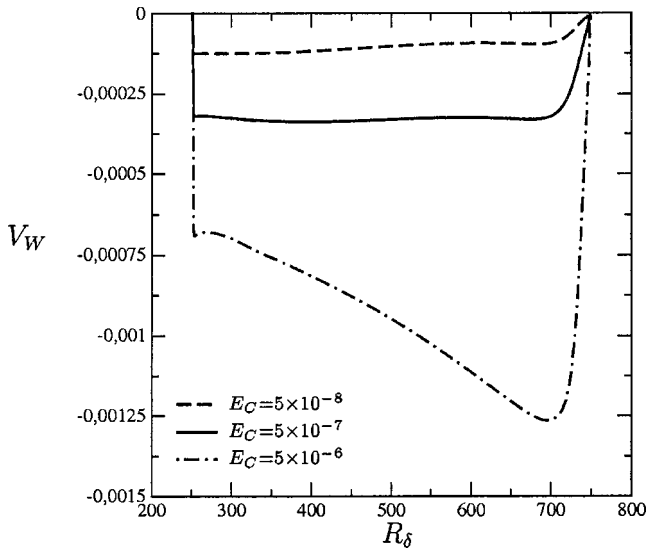

FIG. 10. Optimal suction profiles for different E_C: $F=10^{-4}$, $\Gamma_m=\{x_f\}$, $c_0=0$.

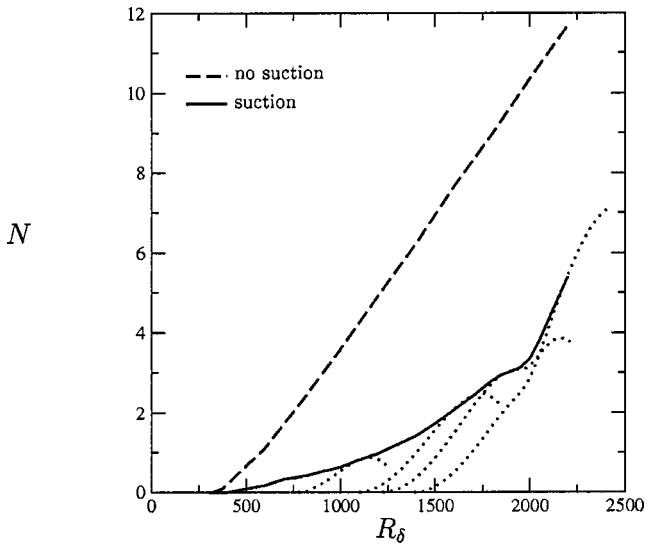

FIG. 12. N factor with and without suction; suction is optimal for $F=2.5\times10^{-5}$, $E_C=2.5\times10^{-7}$. Dashed lines show N for a given F, the solid line is their envelope.

applications a number of external factors (free-stream turbulence, impinging insects, imperfectly operating suction systems, icing, etc.) will be responsible for deviations between the control laws imposed and those actually realized.

Clearly, optimal suction distributions could be determined for any value of F. It is, however, interesting to study the effect of the optimal suction obtained for a given F on instability waves characterized by different values of F. This appears to be necessary in particular in view of the procedure employed; in fact, since the PSE are not uniformly valid in x (just like the Orr–Sommerfeld equation), different starting points need to be employed when integrating the system forward for varying frequencies F. This poses a difficulty if one were interested in computing the control to an inflow condition with a broad frequency content, since the inhomogeneous term in the adjoint equations would be constituted by terms defined over different domains. Fortunately, the situation is not that desperate, and a control obtained for one given frequency turns out to have a positive effect also on other frequencies. Figures 12 and 13 show the behavior of Tollmien–Schlichting waves at different frequencies, all submitted to the same wall suction, i.e., the optimal suction for $\Gamma_m=\{x_f\}$, $E_C=2.5\times10^{-7}$ and $F=2.5\times10^{-5}$. Control begins at $R_\delta=250$ and ends at $R_\delta=2000$. The range of frequencies considered goes from $F=2\times10^{-5}$ to $F=27\times10^{-5}$. For all these frequencies a reduction of the disturbance energy is observed, as shown by the evolution of the N factor with and without suction in Fig. 12. When suction ends, the behavior of N becomes similar to that of the uncontrolled case. If transition were defined by an N value equal to 7, it can be argued that transition would not occur in the domain considered. In Fig. 13 the neutral curves with and without the previous control are displayed. When suction is applied branch I moves downstream and branch II upstream,

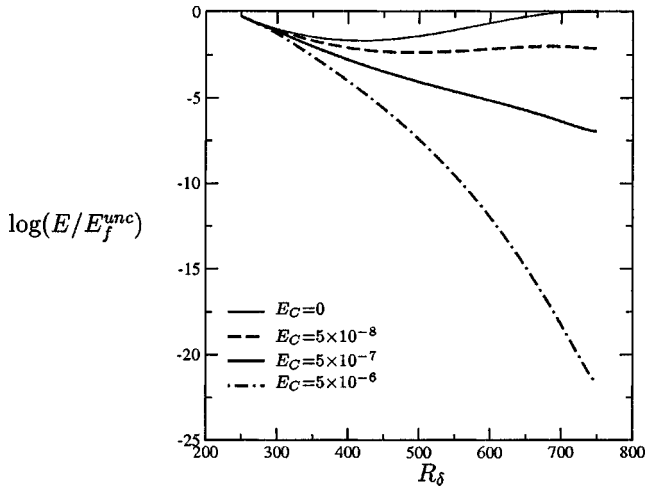

FIG. 11. Optimal disturbance energies for different E_C: $F=10^{-4}$, $\Gamma_m=\{x_f\}$, $c_0=0$.

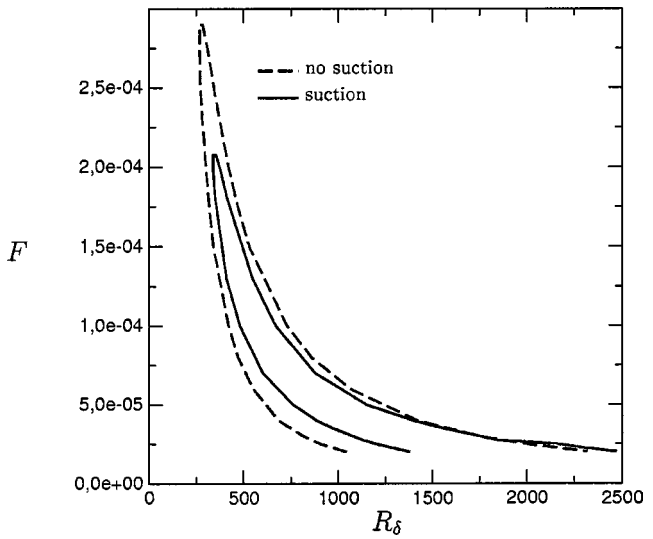

FIG. 13. Neutral curves with and without suction; suction is optimal for $F=2\times10^{-5}$, $E_C=2.5\times10^{-7}$.

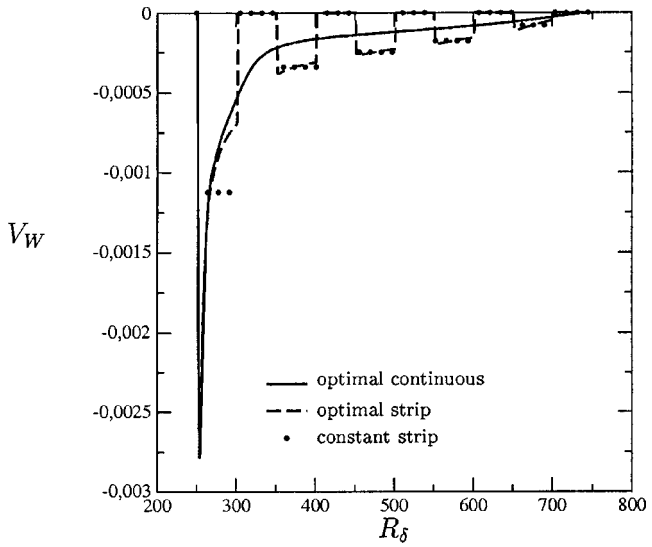

FIG. 14. Suction profiles: continuous suction compared to suction over five strips, $F=10^{-4}$, $E_C=5\times10^{-7}$, $\Gamma_m=\Gamma_C$.

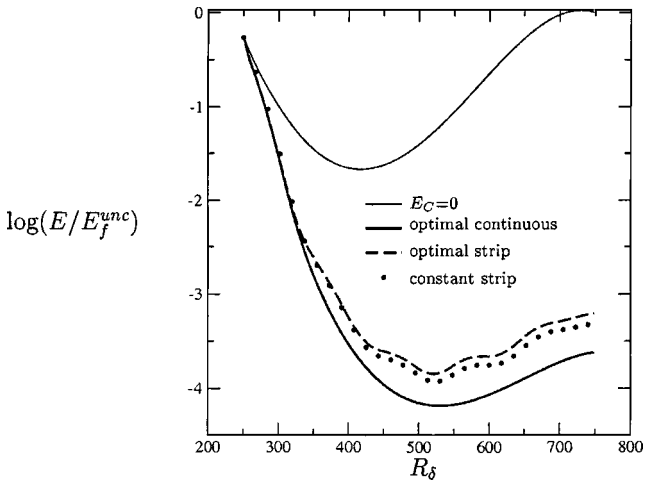

FIG. 15. Disturbance energies: continuous suction compared to suction over five strips.

except for R_δ greater than 1500 where the two second branches are more or less superposed. Globally when suction is applied the unstable region is reduced. The results are less encouraging if the optimal control corresponding to a frequency $F=2\times10^{-4}$ were employed, since the unstable region for that frequency is very small compared to the unstable region for the wave of frequency $F=2.5\times10^{-5}$ (cf. Fig. 13). An empirical observation is that the best control over a wide range of frequencies is the optimal distribution that corresponds to the monochromatic wave displaying the widest unstable range.

A further test consists in considering a control over panels of fixed length; the level of each suction is found by applying the theory to a forcing domain subdivided into several intervals (Fig. 14), with $E_C=5\times10^{-7}$ and $F=10^{-4}$. Here again, not much difference can be seen on the energy curves when comparing "the optimal strip case" to the "constant strip case" (the latter being defined by a constant velocity along each one of the five strips considered producing the same flow rate as the "optimal strip case"). Moreover, even thought the decrease in energy is not as strong as in the continuous case, the reduction is still very significant when compared to the situation without control (Fig. 15). Comparing the energy curves for the two cases with suction over strips, one may think that the constant suction distribution is more efficient than the optimal one. In fact, the mean value of the disturbance energy is smaller for the optimal case, since suction acts more efficiently near the entrance of the control domain.

VI. AN ALTERNATIVE FORMULATION

In the following the problem is reconsidered with an alternative cost functional leading to a much simpler formulation. The reason for trying a simpler approach stems from the observation that suboptimal suction distributions produce satisfactory results (cf. Fig. 12). As discussed in Sec. I even a small decrease of the shape factor is associated with a stabilization of the boundary layer; hence, rather than seeking the optimal suction for damping a Tollmien–Schlichting wave, the objective here is to find the suction profile that will produce the smallest shape factor throughout the domain. This is clearly a heuristic approach; the appropriateness of the results will have to be checked *a posteriori* by performing PSE calculations on the base flow determined.

A. The optimal control system

For this new problem, the state function is the mean flow $\mathbf{Q}$ and the constraint is simply the Prandtl problem, with an (unknown) inhomogeneous wall condition. The new objective functional is the integral of the shape factor H over the objective domain Γ_m, i.e.,

$$\mathcal{J}_0=\int_{\Gamma_m} H\,dx$$

with

$$H=\frac{\delta_1}{\delta_2}=\frac{\int_0^{+\infty}(1-U)dy}{\int_0^{+\infty}U(1-U)dy}.$$

No penalty on the gradient of the velocity suction is added; the influence of such a penalization on the results (in term of suction velocity slope, disturbance growth rate, control energy distribution) is expected to be qualitatively of the same kind as in Sec. V.

Reapplying the methodology described before, the Lagrangian functional $\mathcal{L}$ is defined by

$$\mathcal{L}=\mathcal{J}_0-\mathcal{J}_1,$$

where $\mathcal{J}_1$ is now $\mathcal{J}_1=\langle\mathbf{Q}^*,\mathcal{L}_P\mathbf{Q}\rangle+\int_{x_0}^{x_f}\lambda^*[V(x,0)-V_W(x)]dx+\beta_W^*(E_C-\int_{\Gamma_m}V_W^2\,dx)$. Construction of the optimal control problem is simpler than in the previous case and leads to an optimality system which reads in symbolic notations

$$\mathcal{L}_P\mathbf{Q}=\mathbf{0},$$

$$\mathcal{L}_P^*\mathbf{Q}^*=\mathbf{S}_H^*.$$

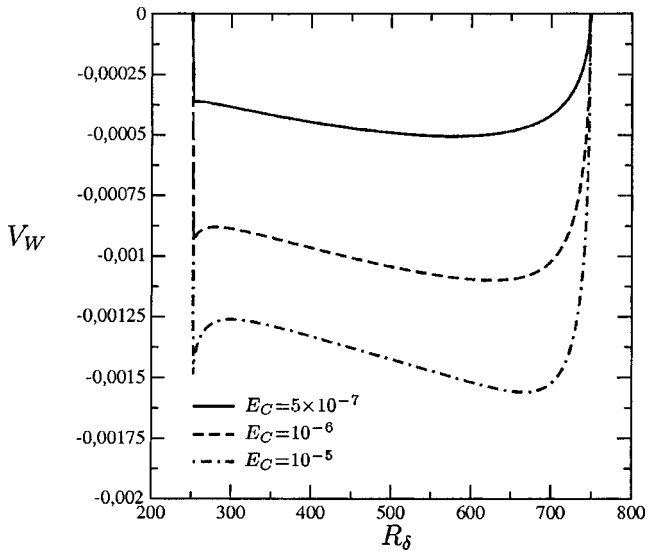

FIG. 16. Minimization of the shape factor: suction profiles for different values of E_C.

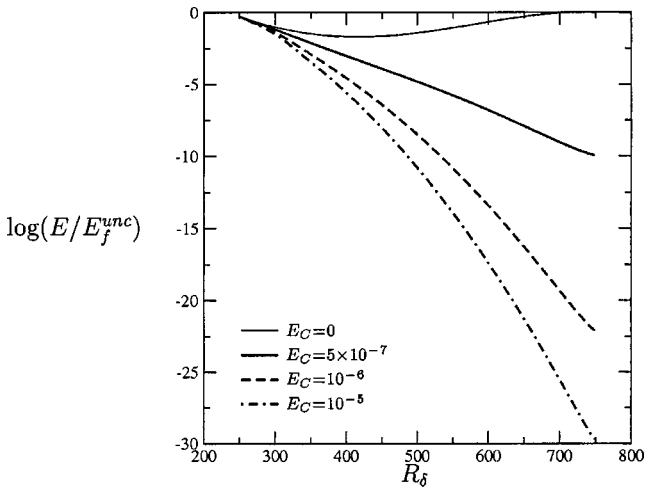

FIG. 18. Optimal disturbance energies for different E_C, $F=10^{-4}$.

The source term $\mathbf{S}_H^*$ of the adjoint problem comes from deriving the cost functional with respect to the mean flow velocity U. Details of the direct and adjoint problems are given in Appendix C.

B. Numerical results

In the following numerical results are given for a control domain that starts at $R_\delta(x_0)=250$ and stops at $R_\delta(x_f)=750$. Figure 16 shows optimal suction profiles for various control energy levels varying from 5×10^{-7} to 10^{-5}. When the control energy is low, suction increases slowly and reaches its maximum near the end of the domain. The result is not very different from those plotted in Figs. 3 and 6. The shape factors are plotted in Fig. 17. Compared to the uncontrolled case, H is reduced over the whole domain and its minimum can be found in correspondence to the maximum amplitude of the wall suction velocity. As the level of E_C increases, a peak appears on the suction distribution at the first station. This sudden peak causes a rapid reduction of H at the entrance of the domain. The effect on a TS wave with $F=10^{-4}$ of the optimal base flow profiles is shown in Fig. 18: as expected, all of these suction distributions induce very significant reductions in disturbance energy.

The two last Figs. (19 and 20) show the behavior of TS waves in a range of frequencies from 2×10^{-5} to 27×10^{-5}. All of these perturbations are subject to the optimal suction computed in the interval $R_\delta(x_0)=250$ to $R_\delta(x_f)=2000$, for $E_C=2.5\times10^{-7}$. The difference between the two neutral curves (Fig. 19) is not large, albeit comparable to that displayed in Fig. 13. On the other hand, the N factor (Fig. 20) is kept below 2 throughout the control domain; past $R_\delta=2000$, N increases in a similar manner as in Fig. 12.

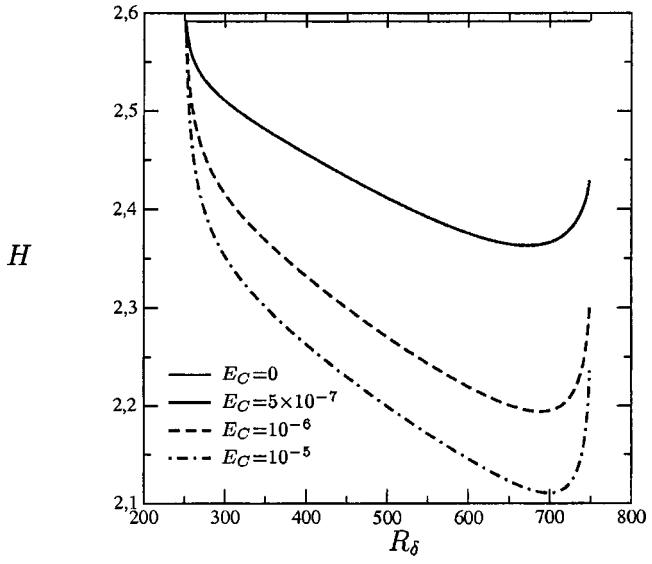

FIG. 17. Optimal shape factors for different E_C.

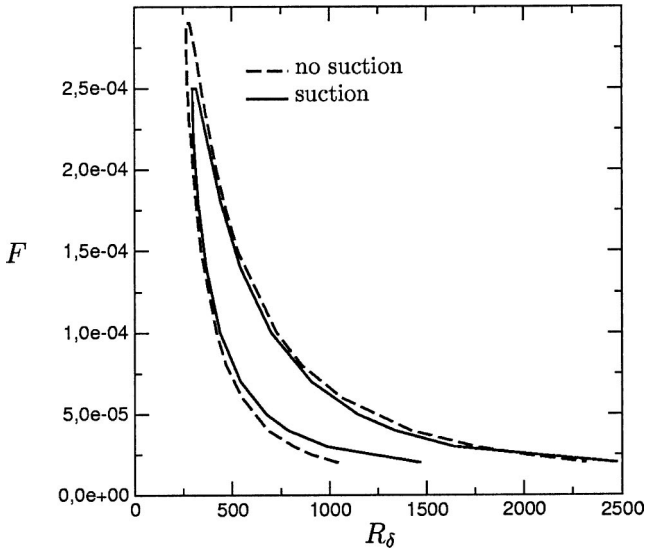

FIG. 19. Neutral curves with and without suction; suction is optimal for $E_C=2.5\times10^{-7}$.

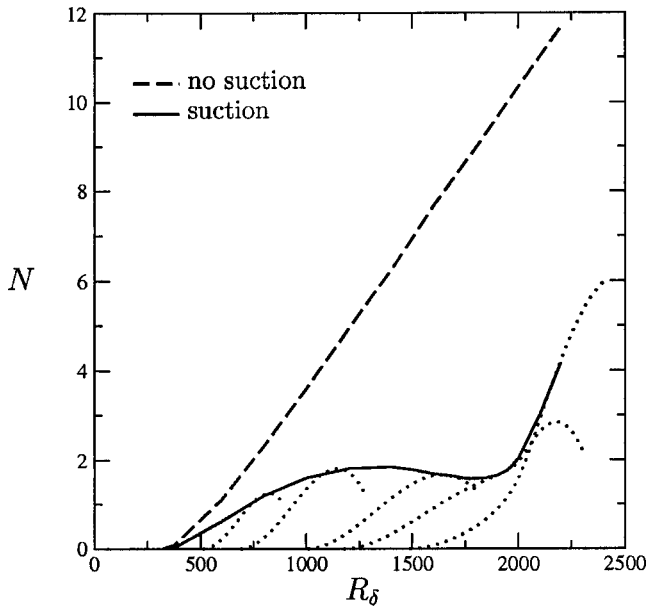

FIG. 20. N factor with and without suction; suction is optimal for $E_C = 2.5\times10^{-7}$.

VII. CONCLUDING REMARKS

The optimal LFC of TS waves developing in a two-dimensional boundary layer has been studied. The technique used for solving this problem relies on the iterative numerical resolution of a coupled system of direct and adjoint equations, plus an optimality condition. One of the key points of this optimal control approach is the definition of the cost functional. In the present case, given the parabolic nature of the equations governing the system's state, it has been found necessary to penalize the derivative of the control velocity, to avoid steep gradients of V_W which could contradict the hypothesis of slow streamwise variation of the base flow. This is particularly the case when the cost functional is based on the integral of the disturbance energy through the streamwise domain, since in this case a very sharp peak of V_W is always produced at the initial control points, to rapidly bring the disturbance energy to a low value. Penalizing the gradient of V_W results in the formation of more or less wide ''boundary layers'' at the edges of the control domain, as deduced from a simplified analysis of the equations. This technique developed here appears to be very efficient and a simple gradient algorithm permits a convergence of the optimality condition (7) within few iterations, producing large reductions in disturbance energy at mild control cost. When large control energies are employed almost any suction distribution produces strong effects on the TS waves amplitudes, rendering the optimal control approach proposed almost purposeless; on the other hand, the present approach (or a similar one such as that given in Ref. 23) is necessary when a strict constraint exists on the control energy that can be used, or when suction can be applied only over one or a few short porous strips.

An alternative, simpler approach has also been tested based on the minimization of the shape factor. The results are promising for the damping of TS waves.

ACKNOWLEDGMENTS

Several interesting discussions on the topic of this paper have taken place with A. Hanifi, J. Pralits, and other colleagues involved in ALTTA. The financial support of the EU, Contract No. G4RD-CT-2000-00143 ALTTA, with Dr. Dietrich Knörzer as program monitor, is gratefully acknowledged.

APPENDIX A: *A-POSTERIORI* VERIFICATION OF THE PARABOLIC ASSUMPTION USED FOR THE TREATMENT OF THE BOUNDARY LAYER FLOW WITH SUCTION

In some of the cases treated, particularly those for which the penalization parameter s in the cost function is set to zero, the parabolic assumption inherent in Prandtl's equations is put to a rude test, because of the sharp gradients of V_W which can appear (cf. Figs. 3, 6, 8, and 14). Some Navier–Stokes calculations of the boundary layer flow with or without suction have thus been carried out, to assess whether the Prandtl-based numerical predictions are reliable.

The computations reported in the following have been carried out with the JADIM code presented in detail in previous studies to which the reader is referred.[35–37] The code solves the three-dimensional unsteady Navier–Stokes equations written in velocity-pressure variables in a general system of orthogonal curvilinear coordinates. The discretization makes use of a staggered mesh and the equations are integrated in space using a finite volume method, all spatial derivates being approximated using second-order centered schemes. Time advancement is achieved through a Runge–Kutta–Nicolson algorithm which is second-order accurate in time, while incompressibility is enforced at the end of each time step by solving a Poisson equation for an auxiliary potential.

Several different boundary conditions are imposed on the boundaries of the computational domain. In the computations the wall is located at $y=0$ and starts at $x=0$. A uniform inflow velocity $U_\infty=1$ is imposed at $x=x_0<0$, and a parabolic approximation of the governing equations, allowing the flow to leave freely the domain without inducing significant perturbations, is imposed downstream, i.e., for $x=x_f$. On the external boundary, corresponding to $y=y_\infty$, the boundary condition states that the normal derivative of the normal velocity is zero and the tangential velocity equals the uniform inflow velocity. Finally, a symmetry condition is imposed at $y=0$ between the inlet and the beginning of the wall. The reason to initiate the computations ahead of the leading edge (of a zero thickness flat plate) is to allow a ''natural'' adjustment of the flow around the plate's leading edge, a known source of problems in this kind of computation.

The computational domain along y goes from 0 to $y_\infty = 36.8\ \delta(x_f)$, where $\delta(x)=(x\nu/U_\infty)^{1/2}$ and x_f is the rightmost point in the domain. In the streamwise direction the domain ranges from $x_0=-7.1\ \delta(x_f)$ to $x_f=845\ \delta(x_f)$, so that, at the final point, $R_\delta=845$. To ensure grid-converged results several different grids have been tested. Eventually, it is found that a grid composed by 1200×80 nodes is suffi-

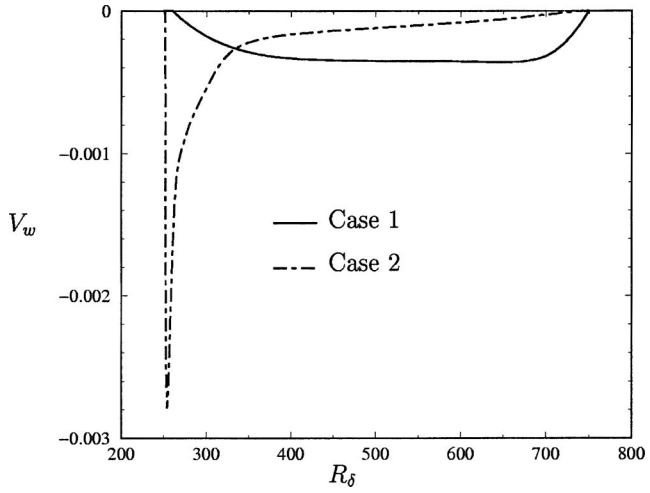

FIG. 21. Suction velocity for cases 1 and 2.

ciently accurate for our purposes. A constant spacing of grid points along the x direction is used, whereas in the y direction the mesh is uniform close to the wall and then smoothly stretched, ensuring that the ratio between the width of two successive cells is less than 1.12. In the absence of control the shape factor found is always within 0.5% of the theoretical value of 2.591, in the range $R_\delta=[200,845]$ (cf. Fig. 24).

The optimal suction distributions chosen for the present comparison tests correspond to $\Gamma_m=\{x_f\}$, $c_0=0.1$ (cf. Fig. 6) and $\Gamma_m=\Gamma_C$, $c_0=0$ (cf. Fig. 8). For both cases we have $E_c=5\times10^{-7}$ and $F=10^{-4}$. These are called cases 1 and 2, respectively, and are displayed in Fig. 21. Case 1 (for which the penalization factor is different from zero) is "well behaved," whereas case 2 is characterized by a very sharp gradient of V_W at the beginning of the control domain.

With suction, the x-momentum Navier–Stokes equation at the wall reads

$$V_W\frac{\partial U}{\partial y}=-\frac{\partial P}{\partial x}+\frac{1}{\mathrm{Re}}\frac{\partial^2 U}{\partial y^2}.$$

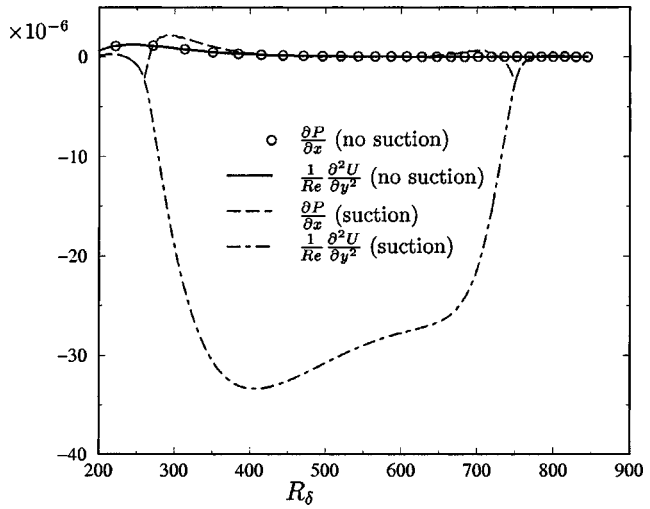

FIG. 22. Wall terms of the streamwise momentum equation at the wall evaluated from Navier–Stokes computations; case without suction and case 1.

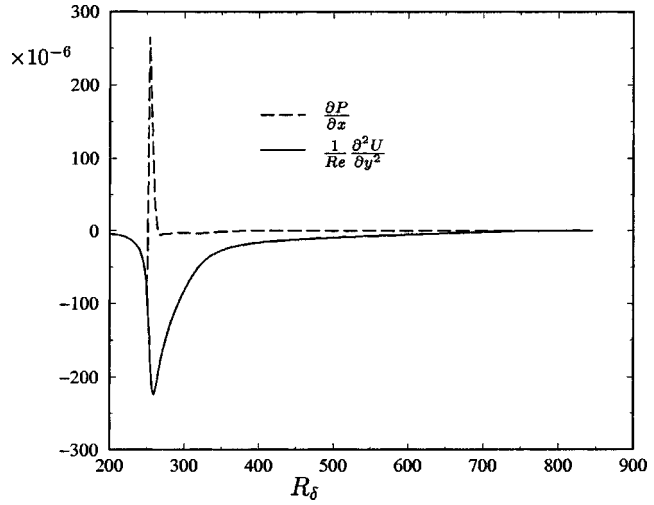

FIG. 23. Wall terms of the streamwise momentum equation at the wall evaluated from Navier–Stokes computations, case 2.

The two terms on the right-hand side of the equation are drawn in Figs. 22 and 23 (the left-hand side term is not shown not to render the figures too crowded; we have, however, verified that the above-mentioned equation is satisfied accurately). In the absence of suction, Fig. 22 shows that the pressure gradient is equal to the viscous term, and they are both less than 0.5×10^{-6}. In case 1, the streamwise pressure gradient can reach the value of 2×10^{-6} in proximity of the point where wall suction is first applied (i.e., $R_\delta=250$). On the other hand, the vertical diffusion term is much larger and it reaches a magnitude of about 3.3×10^{-5}. For case 2 the situation is more critical and a pressure gradient peak can be noticed in Fig. 23 near $R_\delta=250$; both terms of the above-mentioned equation achieve a largest magnitude of about 2.5×10^{-4}. Clearly, near the point where the peak occurs Prandtl's equations are untenable; however, this peak relaxes

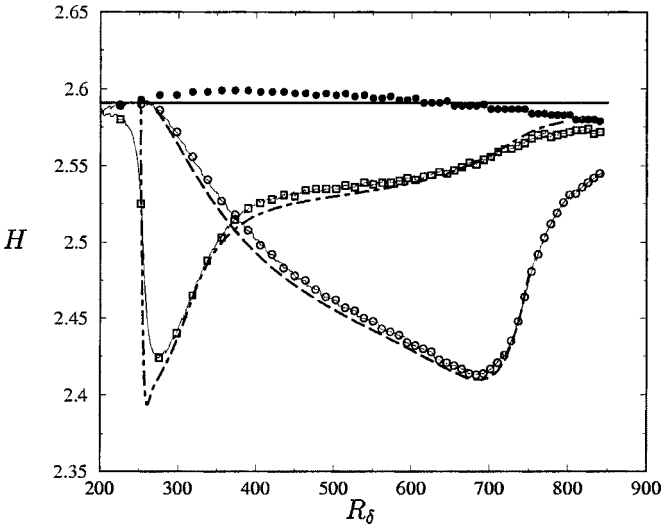

FIG. 24. Shape factors: comparison between the parabolic approach and Navier–Stokes (NS) solutions. Solid line: Blasius's similarity solution. Dashed line: case 1, Prandtl's equations. Dot-dashed line: case 2, Prandtl's equations. Symbols: NS computations corresponding to no suction and cases 1 and 2.

very rapidly and shortly downstream of it $\partial P/\partial x$ becomes very small, consistent with the parabolic approximation. From Fig. 24 it can be appreciated that the agreement in shape factor between Prandtl's and Navier–Stokes' results is very good, even for case 2. This attests to the weak dependence of the shape factor on the mean pressure gradient, for the cases examined here.

Given the very rapid relaxation of the pressure gradient shown in Fig. 23 and the good comparison in shape factors between Prandtl's and Navier–Stokes' solutions, it is reasonable to state that the predictions based on the parabolic model presented in this paper meet the criteria of quality and accuracy required by the present application.

APPENDIX B: OPTIMALITY SYSTEM FOR THE MINIMIZATION OF THE DISTURBANCE ENERGY OF A TS WAVE

1. Direct problem

Direct equations:

$$\begin{bmatrix} 0 & 1 \\ V & -U \end{bmatrix}\mathbf{Q}_y+\begin{bmatrix} 1 & 0 \\ 0 & 0 \end{bmatrix}\mathbf{Q}_x+\begin{bmatrix} 0 & 0 \\ -R_{\delta_0}^{-1} & 0 \end{bmatrix}\mathbf{Q}_{yy}=\mathbf{0},$$

$$\begin{bmatrix} V & 0 & 0 \\ 0 & V & 1 \\ 0 & 1 & 0 \end{bmatrix}\mathbf{q}_y+\begin{bmatrix} U & 0 & 1 \\ 0 & U & 0 \\ 1 & 0 & 0 \end{bmatrix}\mathbf{q}_x+\begin{bmatrix} \xi_0+U_x & U_y & i\alpha \\ 0 & \xi_0-V_y & 0 \\ i\alpha & 0 & 0 \end{bmatrix}\mathbf{q}+\begin{bmatrix} -R_{\delta_0}^{-1} & 0 & 0 \\ 0 & -R_{\delta_0}^{-1} & 0 \\ 0 & 0 & 0 \end{bmatrix}\mathbf{q}_{yy}=\mathbf{0}$$

with $\xi_0=i(\alpha U-\omega)+\alpha^2/R_{\delta_0}$.

PSE normalization condition: $\int_0^{+\infty}(\overline{u}u_x+\overline{v}v_x)dy=0$.

Boundary conditions:

$$\forall x\in[x_0,x_f],\quad U(x,0)=0,$$

$$V(x,0)=\begin{cases} V_W(x), & x\in\Gamma_C \\ 0, & x\notin\Gamma_C \end{cases},$$

$$\forall x\in[x_0,x_f],\quad \lim_{y\to+\infty}U(x,y)=1,$$

$$\forall x\in[x_0,x_f],\quad [u,v](x,0)=[0,0],$$

$$\forall x\in[x_0,x_f],\quad \lim_{y\to+\infty}[u,v](x,y)=[0,0].$$

Initial conditions:

$$\forall y\in[0,+\infty[,\quad U(x_0,y)=U_0(y),$$

$$\forall y\in[0,+\infty[,\quad [u,v,p](x_0,y)\chi(x_0)=[u_0,v_0,p_0](y),$$

with U_0 the Blasius solution at x_0 and $[u_0,v_0,p_0]$ the corresponding eigensolution.

2. Adjoint problem

Adjoint equations:

$$\begin{bmatrix} 1 & -U \\ 0 & V \end{bmatrix}\mathbf{Q}_y^*+\begin{bmatrix} 0 & 0 \\ 1 & 0 \end{bmatrix}\mathbf{Q}_x^*+\begin{bmatrix} 0 & -2U_y \\ 0 & 2V_y \end{bmatrix}\mathbf{Q}^*+\begin{bmatrix} 0 & 0 \\ 0 & R_{\delta_0}^{-1} \end{bmatrix}\mathbf{Q}_{yy}^*=\mathbf{S}^*,$$

$$\begin{bmatrix} V & 0 & 0 \\ 0 & V & 1 \\ 0 & 1 & 0 \end{bmatrix}\mathbf{q}_y^*+\begin{bmatrix} U & 0 & 1 \\ 0 & U & 0 \\ 1 & 0 & 0 \end{bmatrix}\mathbf{q}_x^*+\begin{bmatrix} \xi_1-V_y & 0 & i\overline{\alpha} \\ -U_y & \xi_1+V_y & 0 \\ i\overline{\alpha} & 0 & 0 \end{bmatrix}\mathbf{q}^*+\begin{bmatrix} R_{\delta_0}^{-1} & 0 & 0 \\ 0 & R_{\delta_0}^{-1} & 0 \\ 0 & 0 & 0 \end{bmatrix}\mathbf{q}_{yy}^*=\mathbf{s}^*$$

with

$$\xi_1=i(\overline{\alpha}U-\omega)-\frac{\overline{\alpha}^2}{R_{\delta_0}},$$

$$\mathbf{S}^*=2\,\mathrm{Real}\begin{bmatrix} \overline{u}^*u_y+\overline{v}^*v_y \\ i\alpha(\overline{u}^*u+\overline{v}^*v)+\overline{v}^*v_x+\overline{u}^*u_x+(\overline{v}^*v-\overline{u}^*u)_x-(\overline{u}^*v)_y \end{bmatrix},$$

$$\mathbf{s}^*=\begin{cases} \begin{bmatrix} \overline{\gamma}^*u_x-(\gamma^*u)_x-(1-k)u|\chi|^2/E_m^{\mathrm{unc}} \\ \overline{\gamma}^*v_x-(\gamma^*v)_x-(1-k)v|\chi|^2/E_m^{\mathrm{unc}} \\ 0 \end{bmatrix}, & x\in\Gamma_m \\ \begin{bmatrix} \overline{\gamma}^*u_x-(\gamma^*u)_x \\ \overline{\gamma}^*v_x-(\gamma^*v)_x \\ 0 \end{bmatrix}, & x\notin\Gamma_m \end{cases}.$$

Adjoint PSE closure relation:

$$\frac{dJ}{dx}(x)=\begin{cases}(k-1)/E_m^{\mathrm{unc}}\chi\overline{\chi}\displaystyle\int_0^{+\infty}(\overline{u}u+\overline{v}v)dy, & x\in\Gamma_m\\ 0, & x\notin\Gamma_m\end{cases}$$

with

$$J(x)=\int_0^{+\infty}\left[\left(U-\frac{2i\alpha}{R_{\delta_0}}\right)(\overline{u}^*u+\overline{v}^*v)+\overline{u}^*p+\overline{p}^*u\right]dy.$$

Boundary conditions:

$$\forall x\in[x_0,x_f],\quad B(x,0)=0,$$

$$\forall x\in[x_0,x_f],\quad \lim_{y\to+\infty}[A,B](x,y)=[0,0],$$

$$\forall x\in[x_0,x_f],\quad [u^*,v^*](x,0)=[0,0],$$

$$\forall x\in[x_0,x_f],\quad \lim_{y\to+\infty}[u^*,v^*](x,y)=[0,0].$$

Terminal conditions:

$$\forall y\in[0,+\infty[,\quad \mathrm{A(xf,y)=0},$$

$$\forall y\in\,]0,+\infty[,$$

$$[u^*,v^*,p^*](x_f,y)=(k|\chi(x_f)|^2-\gamma^*(x_f))\left[0,\frac{v}{U},u\right](x_f,y),$$

$$J(x_f)=\frac{k\chi\overline{\chi}}{E_f^{\mathrm{unc}}}\int_0^{+\infty}(\overline{u}u+\overline{v}v)dy\Bigg|_{x_f},$$

$$\gamma^*(x_f)=\frac{k\chi\overline{\chi}}{E_f^{\mathrm{unc}}}\left.\frac{\displaystyle\int_0^{+\infty}\frac{2i\overline{\alpha}}{R_{\delta_0}U}\overline{v}v\,dy}{\displaystyle\int_0^{+\infty}\left(1+\frac{2i\overline{\alpha}}{R_{\delta_0}U}\right)(\overline{u}u+\overline{v}v)dy}\right|_{x_f}.$$

3. Optimality condition

(with $c_0=0$)

$$A(x,0)=\begin{cases}-2\beta_W^*V_W(x) & x\in\Gamma_C\\ 0 & x\notin\Gamma_C\end{cases}.$$

APPENDIX C: OPTIMALITY SYSTEM FOR THE REDUCTION OF THE SHAPE FACTOR *H*

1. Direct problem

Direct equations:

$$\begin{bmatrix}0&1\\V&-U\end{bmatrix}\mathbf{Q}_y+\begin{bmatrix}1&0\\0&0\end{bmatrix}\mathbf{Q}_x+\begin{bmatrix}0&0\\-R_{\delta_0}^{-1}&0\end{bmatrix}\mathbf{Q}_{yy}=\mathbf{0}.$$

Boundary conditions:

$$\forall x\in[x_0,x_f],\quad U(x,0)=0,$$

$$\forall x\in[x_0,x_f],\quad \lim_{y\to+\infty}U(x,y)=1,$$

$$V(x,0)=\begin{cases}0, & x\notin\Gamma_C\\ V_W(x), & x\in\Gamma_C\end{cases}.$$

Initial condition:

$$\forall y\in[0,+\infty[,\quad U(x_0,y)=U_0(y).$$

2. Adjoint problem

Adjoint equations:

$$\begin{bmatrix}1&-U\\0&V\end{bmatrix}\mathbf{Q}_y^*+\begin{bmatrix}0&0\\1&0\end{bmatrix}\mathbf{Q}_x^*+\begin{bmatrix}0&-2U_y\\0&2V_y\end{bmatrix}\mathbf{Q}^*+\begin{bmatrix}0&0\\0&R_{\delta_0}^{-1}\end{bmatrix}\mathbf{Q}_{yy}^*=\frac{1}{\delta_2}\begin{bmatrix}0\\1+H(1-2U)\end{bmatrix}.$$

Boundary conditions:

$$\forall x\in[x_0,x_f],\quad B(x,0)=0,$$

$$\forall x\in[x_0,x_f],\quad \lim_{y\to+\infty}[A,B](x,y)=[0,0].$$

Terminal condition:

$$\forall y\in[0,+\infty[,\quad A(x_f,y)=0.$$

3. Optimality condition

$$A(x,0)=\begin{cases}0, & x\notin\Gamma_C\\ -2\beta_W^*V_W(x), & x\in\Gamma_C\end{cases}.$$

[1] R. D. Joslin, "Overview of laminar flow control," NASA/TP-1998-208705, October 1998.
[2] T. Herbert, "Parabolized stability equations," Annu. Rev. Fluid Mech. **29**, 245 (1997).
[3] G. I. Marchuk, *Adjoint Equations and Analysis of Complex Systems* (Kluwer, Dordrecht, 1995).
[4] "Special issue on adjoint systems," edited by A. Bottaro, J. Mauss, and D. S. Henningson, Flow, Turbul. Combust. **65** (3/4) (2000).
[5] H. Schlichting, "Die grenzschicht mit absaugung und ausblasen," Luftfahrtforschung **19**, 179 (1942).
[6] J. T. Stuart, "Hydrodynamic stability," in *Laminar Boundary Layers*, edited by L. Rosenhead (Dover, New York, 1988).
[7] H. Schlichting, *Boundary-Layer Theory* (McGraw–Hill, New York, 1979).
[8] R. D. Joslin, M. D. Gunzburger, R. A. Nicolaides, G. Erlebacher, and M. Y. Hussaini, "Self-contained automated methodology for optimal flow control," AIAA J. **35**, 816 (1997).
[9] M. D. Gunzburger, "Introduction into mathematical aspects of flow control and optimization, von Karman Institute for Fluid Dynamics," Lecture Series 1997-05 Inverse Design and Optimization Methods, 21–25 April 1997.
[10] P. Cathalifaud and P. Luchini, "Algebraic growth in a boundary layer: Optimal control by blowing and suction at the wall," Eur. J. Mech. B/Fluids **19**, 469 (2000).
[11] S. Walther, C. Airiau, and A. Bottaro, "Optimal control of Tollmien–Schlichting waves in a developing boundary layer," Phys. Fluids **13**, 2087 (2001).
[12] C. Airiau, S. Walther, and A. Bottaro, "Boundary layer sensitivity and receptivity," C. R. Mecanique **330**, 259 (2002).
[13] A. Tumin and A. V. Fedorov, "Instability wave excitation by a localized vibrator in the boundary layer," J. Appl. Mech. Tech. Phys. **25**, 867 (1984).
[14] A. Tumin, "Receptivity of pipe Poiseuille flow," J. Fluid Mech. **315**, 119 (1996).
[15] D. C. Hill, "Adjoint system and their role in the receptivity problem for boundary layer," J. Fluid Mech. **292**, 183 (1995).
[16] D. C. Hill, "Receptivity in non-parallel boundary layers," FEDSM97-3108, ASME Fluids Engineering Division Summer Meeting, 1997.

[17]P. Luchini and A. Bottaro, ''Görtler vortices: A backward-in-time approach to the receptivity problem,'' J. Fluid Mech. **363**, 1 (1998).
[18]C. Airiau, S. Walther, and A. Bottaro, ''Non-parallel receptivity and the adjoint PSE,'' in *IUTAM Symposium on Laminar-Turbulent Transition, Sedona, AZ, September 1999*, edited by H. F. Fasel and W. S. Saric (Springer, New York, 2000), p. 57.
[19]S. Collis and A. Dobrinsky, ''Evaluation of adjoint based methods for the prediction of the receptivity,'' in Ref. 18, p. 111.
[20]A. Dobrinsky and S. Collis, ''Adjoint parabolized stability equations for receptivity prediction,'' AIAA Pap. 2000–2651 (2000).
[21]J. Pralits, C. Airiau, A. Hanifi, and D. S. Henningson, ''Sensitivity analysis using adjoint parabolized stability equations for compressible flows,'' Flow, Turbul. Combust. **65**, 321 (2000).
[22]C. Airiau, ''Non parallel acoustic receptivity of a Blasius boundary layer using an adjoint approach,'' Flow, Turbul. Combust. **65**, 347 (2000).
[23]P. Balakumar and P. Hall, ''Optimum suction distribution for transition control,'' Theor. Comput. Fluid Dyn. **13**, 1 (1999).
[24]C. Airiau, J. Pralits, A. Bottaro, and A. Hanifi, ''Adjoint PSE and boundary layer equations for HLFC,'' Technical Report No. TR10 on the ALTTA EU project, February 2001.
[25]J. Pralits, A. Hanifi, and D. S. Henningson, ''Adjoint-based optimization of steady suction for disturbance control in incompressible flows,'' J. Fluid Mech. **467**, 129 (2002).
[26]T. Herbert and F. P. Bertolotti, ''Stability analysis of non-parallel boundary layers,'' Bull. Am. Phys. Soc. **32**, 2079 (1987).
[27]F. P. Bertolotti, Ph.D. thesis, The Ohio State University, Colombus, OH, 1991.
[28]C. Airiau, Ph.D. thesis, Ecole Nationale Supérieure de l'Aéronautique et de l'Espace, Toulouse, France, 1994.
[29]P. Andersson, D. S. Henningson, and A. Hanifi, ''On a stabilization procedure for the parabolic stability equations,'' J. Eng. Math. **33**, 311 (1998).
[30]C. Airiau and G. Casalis, ''Boundary layer linear stability using a system of parabolic equations,'' Rech. Aerosp. **5**, 57 (1993).
[31]H. L. Reed, W. S. Saric, and D. Arnal, ''Linear stability theory applied to boundary layers,'' Annu. Rev. Fluid Mech. **28**, 389 (1996).
[32]A. M. O. Smith and N. Gamberoni, ''Transition, pressure gradient and stability theory,'' Report No. ES 26388, Douglas Aircraft Co., El Segundo, CA, 1956.
[33]J. L. Van Ingen, ''A suggested semi-empirical method for the calculation of boundary layer transition region,'' Delft University of Technology, Department of Aerospace Engineering, Report No. UTH-74, 1956.
[34]S. Collis, K. Ghayour, M. Heinkenschloss, M. Ulbrich, and S. Ulbrich, ''Optimal control of unsteady compressible viscous flows,'' Int. J. Numer. Methods Fluids **40**, 1401 (2002).
[35]J. Magnaudet, M. Rivero, and J. Fabre, ''Accelerated flows past a rigid sphere or a spherical bubble. Part I. Steady straining flow,'' J. Fluid Mech. **284**, 97 (1995).
[36]I. Calmet and J. Magnaudet, ''Large-eddy simulation of high Schmidt number mass transfer in a turbulent channel flow,'' Phys. Fluids **9**, 438 (1997).
[37]D. Legendre and J. Magnaudet, ''The lift force on a spherical bubble in a viscous linear shear flow,'' J. Fluid Mech. **368**, 81 (1998).